VOCs catalytic removal over hierarchical porous zeolite NaY supporting Pt or Pd nanoparticles

Rebecca El Khawaja, Shilpa Sonar, Tarek Barakat, Nicolas Heymans, Bao-Lian Su, Axel Löfberg, Jean-Francois Lamonier, Jean-Marc Giraudon, Guy de Weireld, Renaud Cousin, et al.

VOCs catalytic removal over hierarchical porous zeolite NaY supporting Pt or Pd nanoparticles

Rebecca El Khawaja[1], Shilpa Sonar[2], Tarek Barakat[3], Nicolas Heymans[4], Bao-Lian Su[3*], Axel Löfberg[2], Jean-François Lamonier[2*], Jean-Marc Giraudon[2], Guy De Weireld[4], Christophe Poupin[1], Renaud Cousin[1], Stéphane Siffert[1*]

[1] Univ. Littoral Côte d'Opale, U.R. 4492, UCEIV, Unité de Chimie Environnementale et Interactions sur le Vivant, SFR Condorcet FR CNRS 3417, F-59140 Dunkerque, France
[2] Univ. Lille, CNRS, Centrale Lille, Univ. Artois, UMR 8181 – UCCS – Unité de Catalyse et Chimie du Solide, F-59000 Lille, France
[3] Univ. Namur, Namur Institute of Structured Matter (NISM), Laboratory of Inorganic Materials Chemistry, B-5000, Belgium
[4] Univ. Mons, Service de Thermodynamique et de Physique mathématiques, B-7000 Mons, Belgium
* Correspondence: stephane.siffert@univ-littoral.fr; jean-francois.lamonier@univ-lille.fr; bao-lian.su@unamur.be

Highlights

- Hierarchical zeolite with bimodal porosity were prepared by post-treatment (desilication, dealumination and acid washing).
- Post-synthesis treatments can affect the textural properties damaging zeolite structures.
- Different dispersion aspect for Pd and Pt particles is revealed since the bimodal porosity (NaY_{mod}) promotes a better surface dispersion of Pt particles while Pd is detected on the surface and in the pore structure.
- Pt-based catalysts exhibit better catalytic performances than Pd-based samples for ethanol and toluene total oxidation.

Abstract:

The present work reports the impregnation of palladium (Pd) or platinum (Pt) on hierarchical porous zeolite catalysts for Volatile Organic Compounds (VOCs) oxidation. The hierarchical porous zeolite (NaY_{mod}) was synthesized *via* a top-down approach to incorporate mesoporosity into the microporous zeolite NaY. This process was achieved through a three steps synthesis: dealumination, desilication and alkaline treatment. 0.5 wt% of Pd and Pt precursors were then added to NaY and NaY_{mod} supports by wet impregnation in order to elaborate efficient catalysts for the total oxidation of two types of VOCs, ethanol and toluene, which are probe molecules for oxygenated VOCs and BTEX compounds respectively. The supported and unsupported samples were characterized by X-Ray Diffraction (XRD), N_2-physisorption, Transmission Electron Microscopy (TEM), and X-Ray Photoelectron Spectroscopy (XPS). The modified mesostructured support ensures a better dispersion of the active phases and led to a partial presence of highly reactive Pt(II) species in the case of platinum-based samples. Whatever the oxidation reaction, these latter demonstrate higher conversions compared to palladium-based ones. The presence of Pt(II) species provided a high catalytic performance, with a total degradation of both VOC probe molecules at temperatures lower than 170 °C. Such temperatures have not been recorded before for NaY supported materials.

Keywords: Pt and Pd supported zeolites; Hierarchical porous zeolite; VOCs oxidation

1. Introduction

Volatile organic compounds (VOCs) are the most common forms of air pollutants generated from chemical, petrochemical, pharmaceutical, building materials and printing industries. VOCs can remain in the atmosphere for up to 60 days while affecting directly the human health since some of them are carcinogenic and can alter the body's functions [1–5]. These compounds highly affect the environment since they are the primary causes of photochemical reactions in the atmosphere causing the formation of tropospheric ozone [6,7]. The treatment of air pollution by heterogeneous catalysis involves the development of efficient catalytic systems [8]. The main challenge of such a technology is the development of high-performance catalytic materials recognized for their

efficiency, thermal stability and selectivity. The supported noble metals and transition metal oxides are considered as promising catalysts. Although expensive, noble metals are widely used for catalytic oxidation of VOCs because of their higher catalytic activity and selectivity. They are generally used as active phases supported on porous materials thus ensuring their dispersion on the surface and within the pores [9]. Different types of materials had been used as support such as alumina [10,11], titania [12,13], zirconia [14,15] , zeolites [16–18] and others.

Zeolites are natural or synthetic crystalline aluminosilicates. Their three-dimensional microporous structure is formed by a regular sequence of TO_4 tetrahedra (SiO_4 or AlO_4^-) interconnected by oxygen atoms. The physicochemical properties of zeolites are strongly dependent on the amount of aluminum, represented by the Si/Al ratio. These materials have been widely used as catalysts, adsorbents and ion-exchange materials in the petrochemical industry [19–22]. However, the main restriction of using zeolites is their diffusion limitation resulting from the microporous character of these materials. The micropores also favor the formation of coke during the reaction, thus enhancing the deactivation of the zeolite. Therefore, the synthesis of hierarchical zeolites with a large pore size distribution is considered the best approach to overcome the problems above [23–25]. This should eliminate the mass diffusion limitations on chemical reaction and mass transfer problem inside the network of the zeolite. A better accessibility of the active sites will be ensured thus affecting the catalytic performance of the zeolitic materials [24,26]. Two approaches are the most frequently followed in order to synthesize hierarchically structured zeolites. In the bottom-up strategy, the zeolite synthesis gel contains mesopore inducing agents such as resins, carbon and organic templates. Mesopores are formed simultaneously with the crystalline phase of the zeolites. However, these costly templates require high temperature combustion to be removed from the structure which can be an issue for industrial applications [27]. On the other hand, the top-down approach performs post-treatments to introduce a new network of mesopores in the zeolite. Such an approach focusses on extracting framework elements by dealumination or desilication [19,21]. These acid-base treatments can be carried out at a suitable cost explaining the industrialization of this approach. Therefore, there has been a growing interest in the top-down approaches in order to develop hierarchical zeolite with different porosity.

Zeolite Y is a three-dimensional zeolite belonging to the faujasite family possessing a Si/Al ratio higher than 1.5 and characterized by a high thermal and chemical stability as well as a cation exchange capacity [26,28]. The aim of this work is to synthesize and investigate highly performing catalysts by combining the advantages of a hierarchical zeolite NaY and noble metal particles for the total oxidation of VOC molecules. These materials are expected to be effective for catalytic oxidation reactions of model VOC compounds such as ethanol and toluene. The materials will also be compared to Pt, Pd exchanged microporous NaY samples to highlight the influence of modifying textural properties of these catalytic supports.

2. Materials and methods

2.1 NaY hierarchical zeolite

The microporous zeolite NaY (CBV100; Si/Al = 2.7) was purchased from Zeolyst. Post-synthetic treatments enable the incorporation of mesopores into the zeolite mineral structure by exposing it to acid and base treatments. A three steps synthesis is needed in order to modify the structure of the NaY while adding mesoporosity. Hierarchically structured zeolite Y was synthesized following Verboekend previous studies [19]:

- Dealumination: This process ensures a mild extraction of Al from the Y framework while maintaining its intrinsic crystallinity. 6.7 g of parent zeolite were mixed with 100 mL of H_4EDTA (0.11 $mol.L^{-1}$, Sigma-Aldrich, 98%) at 100 °C for 6 h under reflux. The resulting solution was then filtered and washed with distilled water. The resulting cake was dried overnight at 80 °C.
- Alkaline treatment: The desilication process consists in mixing the dealuminated material with 0.2 $mol.L^{-1}$ NaOH (Roth, 98 %) solution at 50 °C for 30 min under reflux (3.3 g zeolite per 100mL NaOH). The solution was filtered, washed with distilled water and then dried overnight at 80 °C.
- Acid washing: The treated material (6.7 g) was mixed with an aqueous Na_2H_2EDTA solution (0.11 $mol.L^{-1}$, 100 mL, Fisher Scientific, 98 %) in order to remove extra-framework Al from NaY zeolites without affecting the parent zeolite crystals. The solution was maintained at 100 °C for 6 h under reflux and then filtered, washed and dried overnight at 80 °C. The obtained solids will be denoted as **NaY_{mod}** in this work.

A calcination step was performed for the NaY and NaY_{mod} at 450 °C for 5 h (2 $°C.min^{-1}$) under air flow ($L.h^{-1}$). The calcination temperature was selected based on thermogravimetric analysis on the zeolitic supports.

2.2. Catalysts preparation

Noble metal-based catalysts were prepared by wet impregnation of 0.5 wt% Pd and Pt particles on the zeolite supports (NaY and NaY_{mod}). For the Pd based samples, 1.5 g NaY zeolite was suspended in an aqueous palladium (II) nitrate hydrate solution (0.5 $g.L^{-1}$, 99.9 %, Alfa Aesar) with moderate stirring, maintained under reflux for 16 h at 60 °C and then followed by solvent evaporation in a rotavapor at 60 °C (90 rpm, 3 h). As regards the Pt loaded zeolites, a required amount of platinum acetylacetonate salt (0.0107 g, $Pt(C_5H_7O_2)_2$, 97%, Fluka) was added to 50 mL of ethanol and followed by the addition of 1 g of NaY. The suspension was stirred for 16 h at room temperature and followed by solvent evaporation in a rotavapor (100 rpm, 3 h).

Pd and Pt based solids are then dried at 80 °C for 24 h and subsequently calcined under an air flow at 450 °C for 5 h with a heating rate of 2 $°C.min^{-1}$. In order to activate the calcined solids, a reduction step in 5 $\%H_2$ was made prior to each test during 3 h at 300 °C. The synthesized samples were denoted as X/NaY and X/NaY_{mod}, where X represents the noble metal impregnated (Pd; Pt).

2.3. Catalytic evaluation

2.3.1. Total oxidation of ethanol $C_2H_5OH + 3O_2 \rightarrow 2CO_2 + 3H_2O$

The oxidation of ethanol was carried out under atmospheric pressure in a continuous flow fixed-bed reactor (U shape) with 10 mm of internal diameter. The reactor was loaded with 100 mg of catalyst at atmospheric pressure. The catalysts were preactivated before each test at 350 °C for 1 h under flowing air (33 $mL.min^{-1}$). The oxidation reaction takes place under an air flow of 100 $mL.min^{-1}$ with a gas composition of 1000 ppm C_2H_5OH/Air in order to reach a weight hourly space velocity (WHSV) of about 60000 $mL.h^{-1}.g^{-1}$. Inlet and outlet gas streams concentrations were analyzed from 350 °C to 50 °C using a micro-Gas chromatography (Varian CP- 4900) coupled to a Pfeiffer-Vacuum Omnistar Quadrupole Mass Spectrometer (QMS-200).

2.3.2. Total oxidation of toluene $C_7H_8 + 9O_2 \rightarrow 7CO_2 + 4H_2O$

200 mg of the samples were tested for toluene oxidation under atmospheric pressure in a continuous flow fixed bed pyres-glass reactor with inner diameter 10 mm and a wall thickness of 1 mm. Each catalyst was preactivated at 350 °C for 30 min (2 $°C.min^{-1}$) under flowing air (33 $mL.min^{-1}$). The oxidation reaction was studied for 1000 ppm of toluene with a total flow rate of 100 $mL.min^{-1}$. Catalysts performance was evaluated by decreasing the temperature from 350 °C to 50 °C, with a decreasing rate of 0.5 $°C.min^{-1}$ until 150 °C and then 0.2 $°C.min^{-1}$ until 50 °C. The effluents gases were analyzed online by gas chromatography (R3000, SRA Instrument) equipped with a thermal conductivity detector (TCD).

For both reactions, the production of CO_2 (%) should be taken into consideration to avoid erroneous conclusions due to the potential formation of by-products such as acetaldehyde and benzene for ethanol and toluene oxidation, respectively. The production of CO_2 was calculated using the following expression (where z = 2 and 7 for the ethanol and toluene conversion, respectively):

$$CO_2 \text{ production } (\%) = \left(\frac{[CO_2]_{output}}{[VOC]_{input} \times z}\right) \times 100$$

The catalytic activity was calculated at T_{20} considering a plug-flow reactor:

$$A_i = \frac{273.15 \times Q \times [VOC]_0 \times X}{V_M \times T_x \times m \times 10^6 \times wt\%}$$

A_i = Catalytic activity ($mol.h^{-1}.g^{-1}$);
Q = Volume flow ($L.h^{-1}$);
V_M = Molar volume (22.4 $L.mol^{-1}$);
T_X = Catalyst temperature for X % toluene conversion (K);
$[VOC]_0$ = VOC initial concentration (ppm);
X = VOC conversion (%);
m = Catalyst mass (g)
wt% = Metallic weight percentage (%)

2.4. Catalysts characterization

All the calcined materials have been characterized by different physicochemical techniques in order to further understand the impact of the support on the catalytic performances.

The crystallinity of the reduced catalysts and supports were analyzed at room temperature by X-Ray Diffraction (XRD) analysis using a Bruker D8 Advance X-Ray Diffractometer (AXS) equipped with a CuKα radiation (λ = 1.5418 Å) and a Lynx Eye Detector. The measurements were performed from 5° to 80° with a step size Δ(2θ) = 0.02 and a counting time of 2s per step. The degree of crystallinity of all samples was determined by comparing the peaks area of the five most intensive peaks at Bragg angle 2θ between 6 and 35°. The zeolitic supports (NaY and NaY_{mod}) were taken as reference assigning 100 % of crystallinity [29].

Textural properties of all the calcined samples were determined using N_2 adsorption/desorption isotherms carried out using Micromeritics ASAP 2420. Prior to each analysis, the samples were degassed under vacuum for 8 h at 150 °C. The specific surface area was calculated at P/P^o values recorded in the range of 0.05 and 0.25 using the Brunauer Emmett Teller (BET) equation while pore diameter and mesoporous volume were obtained according to Barrett Joyner Halenda (BJH) model. The micropore volume was determined using the Horvath-Kawazoe (HK) method.

Transmission electron microscopy (TEM) images were recorded on a MET FEI Tecnai G2-20 twin microscope equipped with LaB_6 source and providing an electron beam with an acceleration voltage of 200 kV. Samples were deposited on a copper grid without any other treatment.

X-Ray Photoelectron Spectroscopy (XPS) were recorded with a KRATOS, AXIS Ultra spectrometer with a monochromatic Al Kα anode (1486.6 eV) and a hemispherical analyzer with constant ΔE/E. The binding energies (BE) were corrected using the C 1s photopeak at 284.8 eV (due to adventitious carbon species) as an internal standard. Peak fitting was processed with CasaXPS software in order to determine the peak position, height and width.

3. Results and discussion

3.1. Structural properties

The X-ray diffraction patterns of the supports (NaY, NaY_{mod}), as well as impregnated catalysts (Pd, Pt), are displayed in Figure 1.

FIGURE 1

All the diffractograms showed a crystalline FAU framework (JCPDS-ICDD N° 43-0168) corresponding to the typical topological structure of zeolite NaY. No observable change in XRD peak positions, which indicated that the zeolite's structure was well preserved after the addition of mesoporosity and the impregnation of metallic particles. This result was also discussed by other authors, who found that the zeolites can conserve their intracrystalline structure after desilication, dealumination or acid washing [30,31].

The diffraction peaks of the zeolites were too intense, making it difficult to detect of Pd (Pd/PdO) or Pt (Pt/PtO) phases. In order to confirm the presence of crystalline phases in the XRD spectra, a special attention has been attributed to the $32° < 2\theta < 50°$ angle interval for all supported materials. In fact, the designated area includes the diffraction peaks that may be present for Pt (JCPDS-ICDD N 04-0802), PtO (JCPDS-ICDD N° 85-0714), Pd (JCPDS-ICDD N° 46-1043) or PdO (JCPDS-ICDD N° 85-0624). For Pd-based catalysts, no reflections from metallic particles (Pd^0) or oxides (PdO) were observed. This might be related to the fact that these crystalline phases overlap with the peaks of the supporting material at a similar position. Similar results were obtained by Guo et al. who worked on Pd (1 wt%) (and/or Cu) supported on NaY zeolites and showed that no structural modifications were observed on the NaY zeolite for mono- or bimetallic catalysts [32]. On the other hand, the Pt/NaY and Pt/NaY_{mod} slightly showed (111) and (200) lines characteristic of Pt metal at 2θ= 39.8 and 46.4 respectively. The low intensity of the platinum diffraction peaks was due to the low content of Pt (0.5 wt%). Rosso et al. also reported this observation for Pt species dispersed on 3A-type zeolite [33].

The degree of crystallinity for all synthesized samples is reported in List of

Tables

Table 1.

TABLE 1

Each of the NaY and NaY_{mod} were considered as reference for the noble metal supported materials, which derived from it. A greater decrease in the intensities of diffraction peaks was noticed for supported NaY_{mod}-based samples comparing to the NaY materials. Both Pd and Pt samples showed a less crystallized structure resulting from the structural defects generated by the post-synthetic treatments. Therefore, the framework of the zeolite was more affected by the impregnation process when the bimodal porosity was present. Besides, Pd samples had lower crystallinity than Pt samples. This might be related to the type of the precursors used and the synthesis' conditions [34,35].

3.2. Textural properties

N_2-physisorption analysis was used to evaluate pore structures of the zeolite before and after the (i) hierarchization and (ii) the impregnation of noble metals precursors. Figure 2 displays N_2-physisorption isotherms at 77 K of all prepared samples.

FIGURE 2

NaY-based samples exhibited type I isotherms, characteristics of microporous materials according to the IUPAC classification [36]. An increase in the N_2 uptake at low relative pressure (P/P_0) indicated the presence of micropores. In fact, the adsorbed volume increased quickly at low pressure to generate a monolayer, a typical behavior for microporous materials such as zeolites [37]. The isotherms of NaY_{mod} samples displayed mixed characters of type I and type IV confirming the coexistence of micro- and mesostructure in hierarchical NaY_{mod} sample. The hysteresis loop of type H3 indicated the presence of a disordered mesoporosity generated mostly by the alkaline treatment [38,39]. The BET surface area, pore volume (microporous and mesoporous) are listed in

Table *2*.

TABLE 2

The treated zeolite NaY_{mod} showed a slight increase in the specific surface area of the NaY zeolite from 704 to 754 $m^2.g^{-1}$ generated by the modification of the NaY framework after the dealumination and the desilication process. On the other hand, a reduction in the BET surface area was observed after the impregnation of noble metals, except for Pd/NaY. Loaded particles covered the surface of the material which may have possibly caused a partial blockage of the porous structure. The BJH pore size distribution of hierarchical materials was illustrated in the inset of Figure 2. All samples exhibited pore diameters that cover the range of micro- and mesopores. Two different distributions of mesopores were distinguished: one sharp distribution centered at 4 nm and a broader one centered at 8 nm and 10 nm for NaY_{mod} samples. This indicates that the top-down approach generates small and medium-sized mesopores (2-20 nm). Thereby, micropores and mesopores coexist in hierarchical zeolites. Finally, the size of the micropores remained almost unchanged (0.5 nm) for all the samples, which suggested the preservation of NaY microstructure (Figure 1S).

3.3. TEM analysis

TEM images of Pt/NaY, Pt/NaY_{mod}, Pd/NaY, and Pd/NaY_{mod} are shown in Figure 3.

FIGURE 3

The size distribution of platinum and palladium particles is also presented. It has been well known that the particle size of Pt has a crucial influence on the catalytic performance of the Pt-loaded materials [40,41]. As per Figures (a) and (b), it can be shown that Pt nanoparticles were dispersed uniformly in prepared catalysts.

TABLE 3

Platinum particles mean size on NaY_{mod} was relatively similar (3.6 nm) as the one on NaY (4 nm). The observed particle size was in a good agreement with the reported values in literature [42–44]. In the case of Pd/NaY, large particles of Pd have been observed with an average size of 15 nm. In fact, the aqueous medium during the impregnation facilitates the hydrolysis of Pd^{2+} by forming larger particles (clusters) [45]. Furthermore, Pd/NaY_{mod} had a mixture of high and small particles of Pd located on the surface and in the porous structure with mean size 25 and 2.5 nm, respectively. The incorporation of palladium in the pores could be induced by the diffusion or migration of Pd species under the evaporation of water during the synthesis procedure. We can see that the microporous structure was well kept after the post-synthesis treatment on the zeolite, which support the results of the N_2-physisorption explained above. Comparatively, the dispersion of platinum particles on NaY support (33 %) was greater than that of palladium (12 %) (

Table *3*).

3.4. XPS analysis

The surface analysis of Pd and Pt based zeolites materials has been performed by XPS. The direct overlap between Pd $3p_{3/2}$ and O 1s peaks as well as those between Pt $4f_{5/2}$ and Al 2p peaks have been considered. The binding energies of the electrons coming from different core-levels are given in Table 4. For all zeolite samples, the values of binding energies of the electrons coming from O 1s, Si 2p, Al 2p and Na 1s were in agreement with those reported in the literature for zeolites [46–49].

The Pd 3d and Pt 4f regions with well separated spin-orbit components are shown in Figure 4.

FIGURE 4

The Pd 3d region contained a doublet at around 335.0 and 340.2 eV which can be ascribed to Pd $3d_{5/2}$ and Pd $3d_{3/2}$, respectively. Regardless of the support used, the Pd $3d_{5/2}$ photopeak was located at 335 eV (±0.1 eV) indicating that Pd species were in metallic form [50–53]. In fact, the surface analysis did not show a Pd $3d_{5/2}$ peak around 337-338 eV corresponding to palladium in the Pd^{2+} form [53,54]. This result suggested that the palladium precursors used in the preparation were completely converted into metallic particles. Yang et al. also found metallic Pd after calcination under air while studying palladium doped materials treated under different calcination atmosphere (air , N_2 and H_2) [55].

On the other hand, the Pt 4f region was overlapping by Al 2p photopeak. The most intense signal was mainly attributed to Al 2p photopeak while the lowest one was ascribed to Pt $4f_{7/2}$ photopeak. For Pt/NaY sample, the Pt $4f_{7/2}$ photopeak located at BE of 70.6 eV can be attributed to metallic Pt particles [43,56]. For Pt/NaY_{mod} sample, the presence of the metallic platinum was also observed with a Pt $4f_{7/2}$ photopeak at BE of around 71.5 eV. However, the shape of this photopeak was wider in the region of 70-73 eV as compared to the one observed for Pt/NaY sample. This can be explained by the presence of another species of Pt in different oxidation state. The XPS fitting of Pt $4f_{7/2}$ region into two components led to the presence of two Pt $4f_{7/2}$ photopeaks at BE of 70.8 eV and 71.9 eV. The Pt $4f_{7/2}$ photopeak located at higher BE is ascribed to the presence of Pt^{2+} species. These species had also been observed by other authors [57,58]. The fitted Pt 4f core lines can be observed in Figure 4 (d) and inset is showing the clear view of different Pt species. Based on XPS fitting, the contribution of Pt^0 and Pt^{2+} has been calculated and was been found to be 60 % and 40 % respectively.

Table *5* shows the surface atomic composition obtained by XPS, after correction with atomic sensitivity factors.

TABLE 5

Catalysts supported on microporous NaY reveal Si/Al surface ratios that are consistent with the total Si/Al value given by the supplier (CBV100, Zeolyst, Si/Al = 2.7). For these two materials, the zeolite had not undergone post-synthesis treatments unlike those supported on hierarchical zeolites. However, the latter showed higher Si/Al ratios which could be explained by the dealumination of the NaY_{mod} support. Ratios of 3.47 and 3.26 were obtained for the solids Pt/NaY_{mod} and Pd/NaY_{mod}, respectively. This trend points to an aluminum depletion of the zeolite surface, slightly more pronounced for platinum-based catalysts. These results could indicate a difference in the types of acid sites present in the catalytic material. The determination of the Pt surface composition is challenging, due to the low intensity of the Pt 4f photopeak and overlap in the Pt 4f and Al 2p core levels, while Pt 4d core level could not be used because of a too low signal/noise ratio. Nevertheless, there was no significant difference in the Pt/(Si+Al) ratio between Pt/NaY and Pt/NaY_{mod} materials. This result suggested similar Pt dispersion regardless the support used which confirmed the TEM analysis's results. In contrast, the quantification for Pd-loaded materials differed from NaY to NaY_{mod} support. Indeed, the XPS Pd/(Si+Al) ratio was almost four times higher in Pd/NaY than in Pd/NaY_{mod}. This difference suggested that the number of accessible Pd particles was larger than that of Pd/NaY_{mod}. This obtained ratio confirmed the previously dispersion' results of TEM which also revealed that Pd particles were preferentially located at the surface of NaY contrary to those located in the pores of NaY_{mod}.

The metallic weight percentage of Pt or Pd was also deduced from the atomic yield identified by XPS. For example, 0.43 and 0.51 wt% were found for Pt/NaY and Pt/NaY_{mod} samples. This calculation allowed a comparison between the surface composition and the mass composition of the synthesized materials. The latter identified about 0.5 for Pt samples (and 0.4 wt% for Pd ones) by ICP-OES analysis. The results obtained from the XPS were then consistent with those of the ICP-OES, showing a homogeneous dispersion of the particles on the surface of the materials.

3.5. Total oxidation of ethanol

The catalytic activity and selectivity of the supported catalysts towards the total oxidation of ethanol are illustrated on Figure 5.

FIGURE 5

The catalytic performance has been compared in terms of T_{50} and T_{90} which represent the temperatures when 50% and 90% of ethanol was converted into CO_2, respectively. No remarkable improvement in catalytic reaction was noticed between both impregnated catalysts regardless of the porosity of the zeolitic support. Moreover, the catalytic performance depends on the nature of the active phase. Figure 5 shows that Pt based catalysts achieved complete ethanol conversion at lower temperatures than Pd based samples (more than 40 °C difference in the T_{50}). It can be seen that acetaldehyde was the major organic molecule produced as reaction intermediate during ethanol oxidation. According to Figure 5, the selectivity to acetaldehyde was maximum when the CO_2 production was low (around 10%). Other by-products such as ethylene (around 70 ppm for Pt based samples) and diethyl ether (around 5 ppm for Pd based samples) were detected by mass spectrometer. The ethylene was formed after the dissociative adsorption via the rupture of the C-O bond of ethanol. This lead to the formation of ethylene by dehydration of ethanol [10,59]. As for the formation of diethyl ether, Trawczynski reported that for an acidic carrier, the presence of highly acidic sites facilitates the formation of diethyl ether by dehydration of ethanol via ethanol dimerization [60]. When the ethanol conversion was complete, water and CO_2 were the only products emitted.

Comparing the two palladium-loaded catalysts, we notice that Pd/NaY was more active towards high conversions (> 50 %). According to the literature, the activity of palladium is strongly dependent on its particle size and the type of active palladium species. Some studies claim that Pd^{2+} is more active during hydrocarbon combustion reactions [61], but the presence of Pd^0 may also enhance catalyst activity by providing more active sites for VOC dissociation [62]. Others showed that Pd^0 is the most active phase in the catalytic oxidation of VOC [63,64]. Since we obtained Pd^0 for both Pd/NaY and Pd/NaY_{mod} samples then it is mainly the particles sizes that control the catalytic activity [20]. This is consistent with the TEM results presented previously which showed that Pd/NaY had larger particle sizes on the surface than Pd/NaY_{mod}, thus explaining the slight improvement observed. However, the large dispersion of Pd particles inside the micropores of NaY_{mod} disadvantaged the improvement of the catalytic reactivity.

As for platinum-loaded catalysts, the added mesoporosity was not advantageous for supported catalysts. No remarkable improvement of the catalytic reaction between Pt/NaY and Pt/NaY_{mod} has been observed even in the presence of Pt^0 and Pt^{2+} on the surface of Pt/NaY_{mod} (results previously determined by XPS) which according to the literature could ensure a gain in activity. Finol et al. showed that catalytic performances in the presence of Pt^0 provides adsorption sites for VOC and Pt^{2+} allowed the oxidation of this adsorbed molecule into CO_2 and H_2O [13].

3.6. Total oxidation of toluene

Figure 6 shows toluene complete catalytic oxidation *via* light-off curves over Pd- or Pt-impregnated NaY and NaY_{mod}. It represents the light-off curves of all samples, showing the toluene conversion into CO_2 as a function of temperature.

FIGURE 6

It appears that Pt- and Pd-impregnated zeolites led to the complete toluene conversion into CO_2 and H_2O. To compare the catalytic activities, T_{50} and T_{90} were calculated from Figure 6. It is worth mentioning that Pt/NaY and Pt/NaY_{mod} zeolites presented the T_{50} around 104-122 °C lower than Pd/NaY zeolites. Moreover, Pt/NaY_{mod} showed higher catalytic performance than that of Pt/NaY, which could be due to the presence of platinum species in two oxidation states (Pt^0 and Pt^{2+}) as discussed in the XPS results. In addition, the performance of Pt/NaY_{mod} may also be related to the smaller particle size of the Pt species on the hierarchical zeolite, as shown in TEM analysis.

The obtained results suggested that the Pt^0 species were active centers for the total oxidation of toluene into CO_2 and H_2O, in good agreement with reported one [65,66]. T_{90} of toluene was 130 °C over Pt/NaY_{mod} which was 20 °C lower than that (151 °C) of Pt/NaY. This result reveals that Pt/NaY_{mod} possess high amount of catalytically active Pt^0 species, higher Pt dispersion on NaY_{mod}, and good mass transfer compared to Pt/NaY. This might be correlated to the presence of the mesoporosity in Pt/NaY_{mod}. In case of Pd/NaY and Pd/NaY_{mod}, no significant catalytical improvement has been observed. The Pt/NaY and the Pt/NaY_{mod} of this work represented promising candidates comparing to other Pt supported materials (

Table 6). These catalysts showed a better catalytic activity. Taking into consideration the weight percentage of the Pt, the Pt supported on zeolite NaY (presented in this work) showed better activity than those supported on similar silicate based materials (ZSM5, SBA, MCM, etc).

TABLE 6

To summarize, the above results indicate that the post-synthesis treatments of the zeolite in order to add mesoporosity did not effectively improved the catalytic performance of all the samples for both studied probes VOC. No obvious relation between catalytic properties and textural properties can be deduced from the studied materials in this work so far. We suggest that the main effect might be shown in stability tests, where the micro-mesoporous structure may prevent pores blockage by coke deposition. The acidity (number and the strength of the acid sites) of the materials is also very important and may be influencing on the kinetic reaction especially for the ethanol conversion and will be studied in the future. Indeed, the Pt/NaY and the Pt/NaY_{mod} samples of this work represented promising candidates for VOC oxidation.

4. Conclusion

In the present work, the top-down approach was used to incorporate mesoporosity into the microporous structure of the NaY zeolite. After dealumination, desilication and acid treatment, the physicochemical properties of the zeolitic support were modified. The improvement of textural properties was attributed to the introduction of additional mesoporosity into the microporous structures. For both reactions, platinum based samples exhibit much better catalytic performance than palladium ones which was attributed to the existence of more accessible and dispersed particles on the surface. We assume that the dispersion of the palladium particles inside the pores may had cause the non-improvement of the catalytic properties for the total oxidation of the ethanol or the toluene. During toluene total oxidation, the improvement of the catalytic performance of Pt/NaY_{mod} was also related to the presence of Pt^0 and Pt^{2+} species allowing the adsorption of the VOC and its oxidation. Finally, it is necessary to recall the interest that the mesoporous material must have over the lifetime of the catalyst since the formation of coke is preferentially in a microporous system.

Author Contributions: T.B., R.K. and S.S. prepared the materials. T.B., R.K., N.H. and S.S. conducted the experiments. R.K. wrote the first draft of the paper. S.S., J.-F.L., R.C., C.P., G.D.W., J.-M.G., A.L. and B.-L.S. supervised the work. All authors contributed to the data interpretation, the discussion and the revision of the paper.

Funding: The “DepollutAir” project (grant number 1.1.18) of the European Program INTERREG V France-Wallonie-Vlaanderen (FEDER), Région Wallone and Région Hauts-de-France are acknowledged for the funding and their support for this work.

Conflicts of Interest: “The authors declare no conflict of interest.”

List of figures

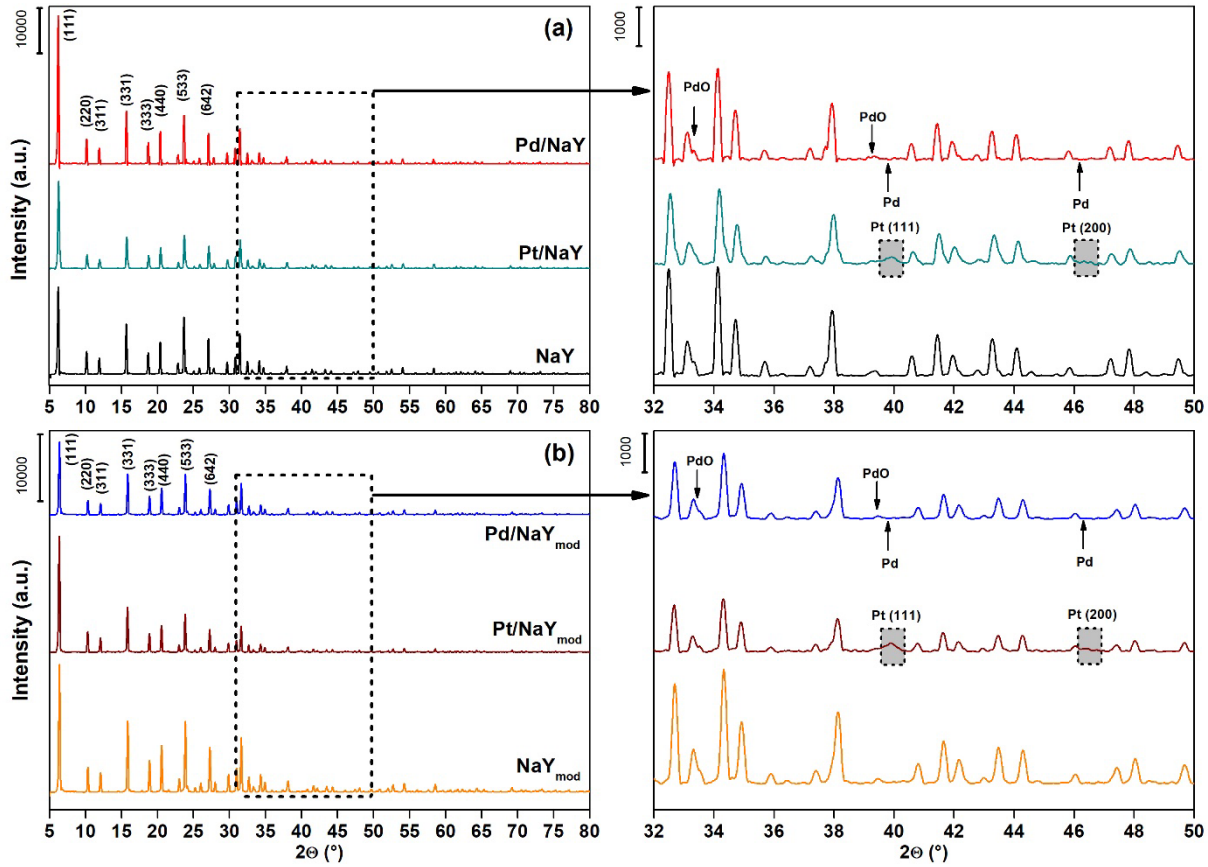

Figure 1. X-ray diffraction patterns of (a) NaY and (b) NaY_{mod} based samples

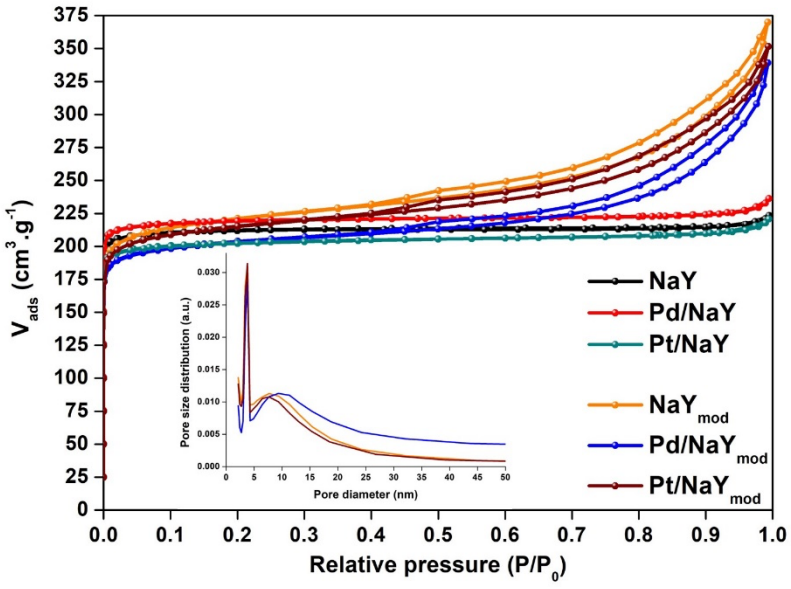

Figure 2. N_2-physisorption isotherms at 77 K of NaY and NaY_{mod} based materials

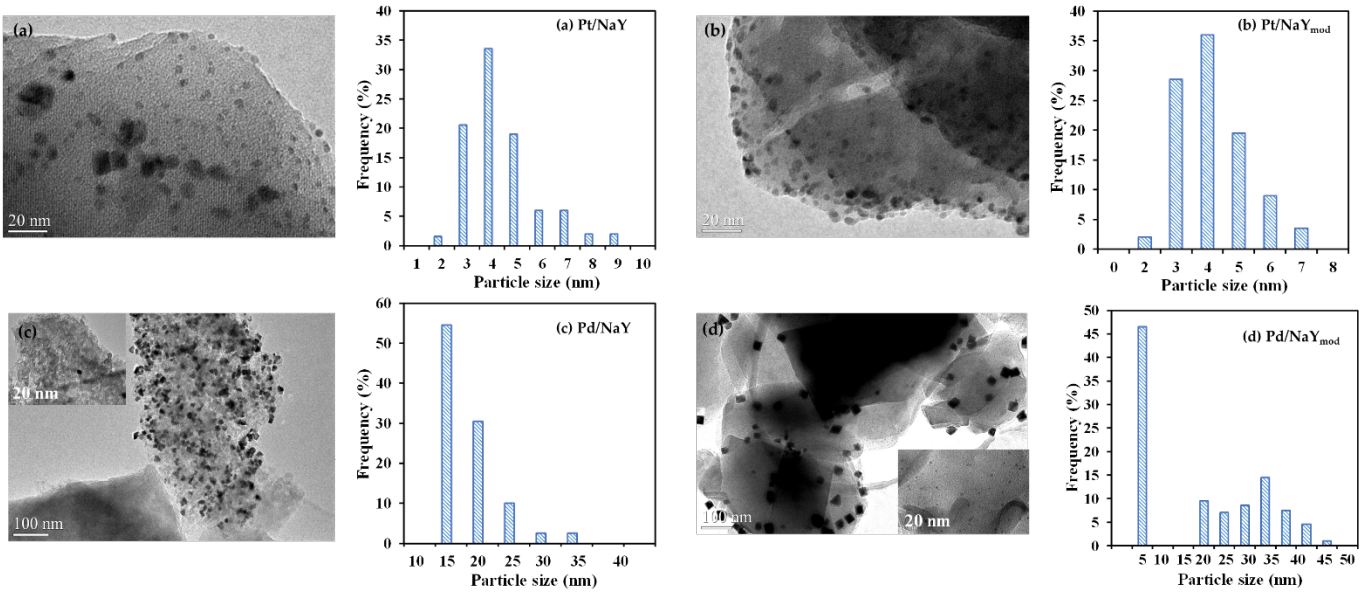

Figure 3. TEM images and size distribution of metallic particles for (a) Pt/NaY, (b) Pt/NaY$_{mod}$, (c) Pd/NaY and (d) Pd/NaY$_{mod}$

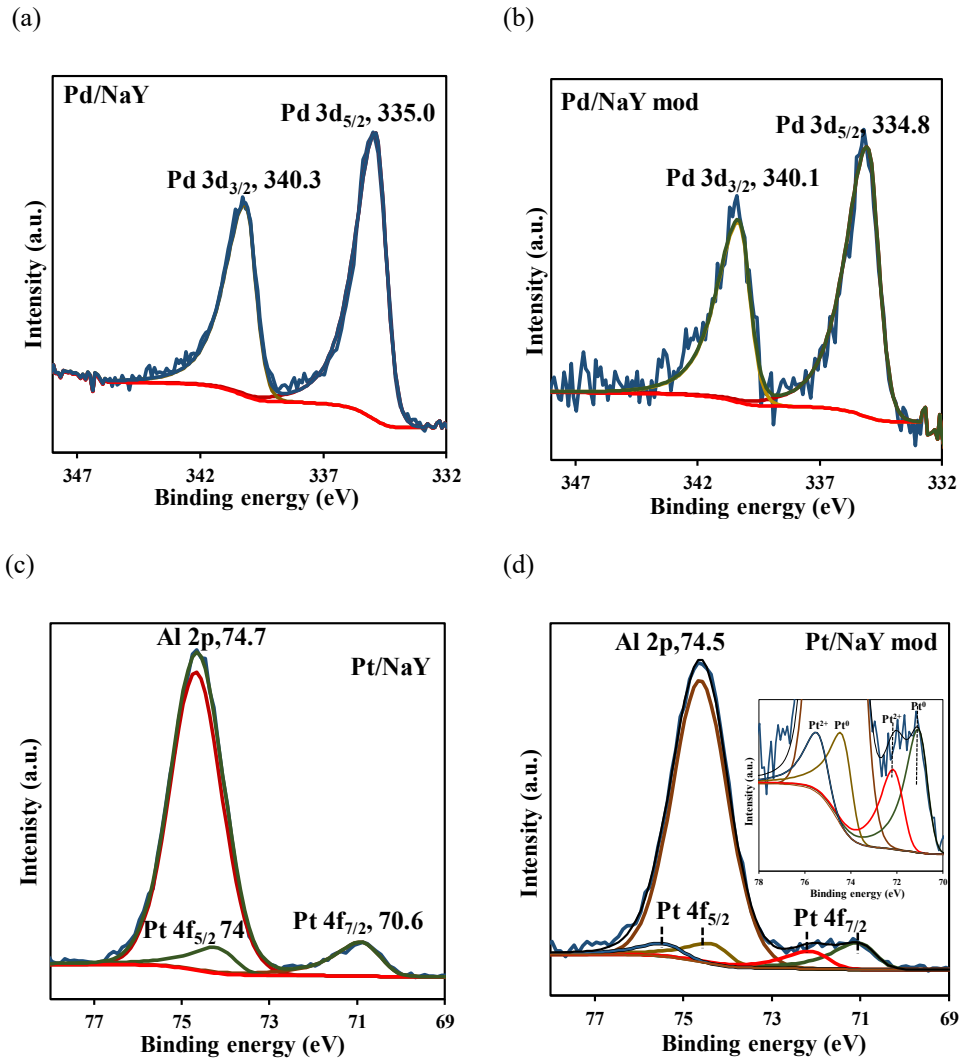

Figure 4. Pd 3d and Al 2p - Pt 4f regions obtained in (a) Pd/NaY, (b) Pd/NaY$_{mod}$, (c) Pt/NaY and (d) Pt/NaY$_{mod}$

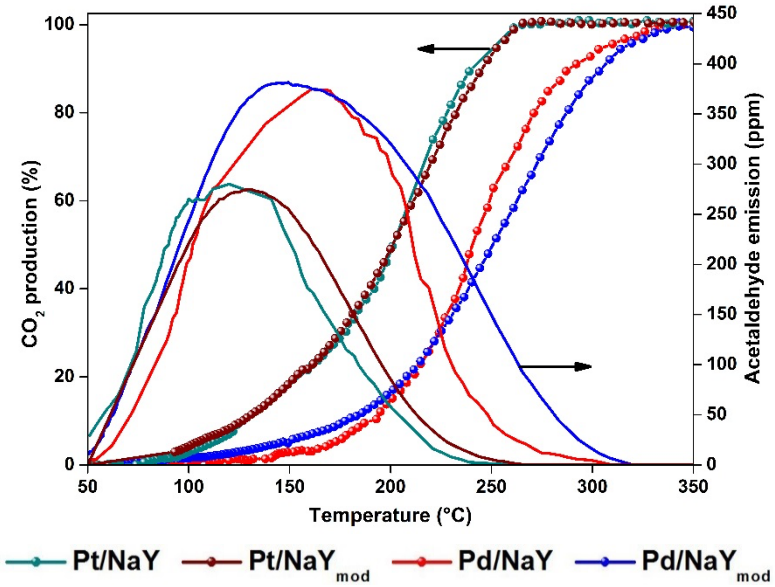

Figure 5. Light-off curves and acetaldehyde emission of ethanol oxidation over Pt/NaY, Pt/NaY$_{mod}$, Pd/NaY, Pd/NaY$_{mod}$

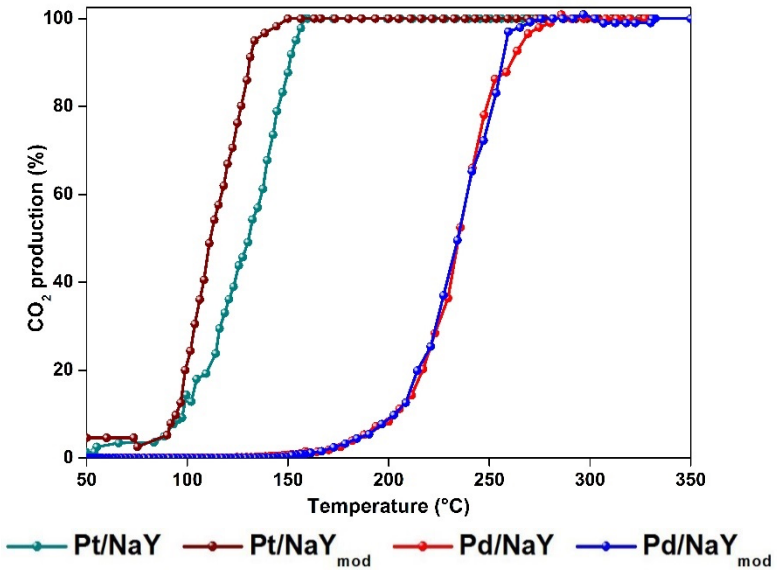

Figure 6. Light-off curves of toluene oxidation over Pt/NaY, Pt/NaY$_{mod}$, Pd/NaY and Pd/NaY$_{mod}$

List of Tables

Table 1. Degree of crystallinity of NaY, NaYmod supports and impregnated metallic catalysts.

Catalysts	**NaY**	**Pt/NaY**	**Pd/NaY**	**NaY_{mod}**	**Pt/NaY_{mod}**	**Pd/NaY_{mod}**
Degree of crystallinity (%)	100	95	94	100	77	64

Table 2. Textural properties of the NaY, NaY_{mod} supports and impregnated metallic catalysts.

Catalysts	**NaY**	**NaY_{mod}**	**Pd/NaY**	**Pd/NaY_{mod}**	**Pt/NaY**	**Pt/NaY_{mod}**
Surface area (m^2/g)[a]	704	754	759	683	686	695
Porous volume (cm^3/g) [b]	0.35	0.57	0.37	0.52	0.34	0.54
Mesoporous volume (cm^3/g)[c]	-	0.26	-	0.22	-	0.23
Microporous volume (cm^3/g)[d]	0.33	0.34	0.34	0.31	0.31	0.33

[a] calculated at P/P_o = 0.05 to 0.25; [b] calculated at P/P_o = 0.99.; [c] calculated using the BJH model using the desorption branch; [d] calculated using the Horvath-Kawazoe method.

Table 3. Size distributions and dispersion of metallic Pt and Pd particles on the zeolitic supports (NaY and NaY_{mod}).

Catalysts	**Pt/NaY**	**Pt/NaY_{mod}**	**Pd/NaY**	**Pd/NaY_{mod}**
Particles mean size (nm)	4	3.6	15	25 and 2.5
Dispersion (%)	33	36	12	7.4 and 44.4

Table 4. Binding energy of electrons from different core levels in Pt or Pd- zeolite based materials.

Catalysts	Binding energy / eV							
	Pt $4f_{5/2}$	**Pt $4f_{7/2}$**	**Pd $3d_{5/2}$**	**Pd $3d_{3/2}$**	**O 1s**	**Al 2p**	**Si 2p**	**Na 1s**
Pt/NaY	74.0	70.6	-	-	532.4	74.7	103.2	1073.1
Pt/NaY_{mod}	75.2 74.1	71.9 70.8	-	-	532.3	74.5	103.1	1072.7
Pd/NaY	-	-	340.3	335.0	532.2	74.5	103.0	1072.5
Pd/NaY_{mod}	-	-	340.2	334.9	532.1	74.5	103.0	1072.4

Table 5. Surface atomic composition of Pt or Pd-zeolite based materials.

Catalysts	Atomic yield (%)								
	Pt	**Pd**	**O**	**Al**	**Si**	**Na**	**Si/Al**	**Pt/(Si+Al)**	**Pd/(Si+Al)**
Pt/NaY	0.04	-	66.8	5.6	15.5	11.9	2.78	0.0019	-
Pt/NaY$_{mod}$	0.05	-	68.5	4.7	16.3	10.4	3.47	0.0024	-
Pd/NaY	-	0.56	67.4	5.6	14.8	11.5	2.64	-	0.027
Pd/NaY$_{mod}$	-	0.16	69.1	4.7	15.3	10.7	3.26	-	0.008

Table 6. Literature survey of toluene catalytic oxidation for Pt supported materials

Catalysts	T_{20} (°C)	Catalytic activity ($mol.h^{-1}.(g\ of\ Pt)^{-1}$)	References
Pt-1.3/ZSM-5	170	2.54×10^{-4}	[43]
Pt-1.5/ZSM-5	160	2.25×10^{-4}	
Pt-1.7/ZSM-5	150	2.03×10^{-4}	
Pt-1.9/ZSM-5	145	1.84×10^{-4}	
Pt-2.1/ZSM-5	150	1.65×10^{-4}	
Pt-2.3/ZSM-5	165	1.45×10^{-4}	
Pt/KZSM-5-60	165	6.68×10^{-5}	[67]
Pt/NaZSM-5-60	175	6.53×10^{-5}	
Pt/NKM-5	178	$3.24*10^{-5}$	[68]
Pt/NKM-5-0.3	187	$3.18*10^{-5}$	
Pt/SBA-15	187	$3.18*10^{-5}$	
Pt/MCM-41	205	$3.06*10^{-5}$	
Pt/NaY	111	$3.81*10^{-4}$	Present work
Pt/NaY_{mod}	99	$3.93*10^{-4}$	

References

[1] V. Soni, P. Singh, V. Shree, V. Goel, Effects of VOCs on human health, in: Energy, Environ. Sustain., 2018: pp. 119–142. http://link.springer.com/10.1007/978-981-10-7185-0_8.

[2] C. Billionnet, D. Sherrill, I. Annesi-Maesano, Estimating the health effects of exposure to multi-pollutant mixture, Ann. Epidemiol. 22 (2012) 126–141. https://doi.org/10.1016/j.annepidem.2011.11.004.

[3] C. Méausoone, R. El Khawaja, G. Tremolet, S. Siffert, R. Cousin, F. Cazier, S. Billet, D. Courcot, Y. Landkocz, In vitro toxicological evaluation of emissions from catalytic oxidation removal of industrial VOCs by air/liquid interface (ALI) exposure system in repeated mode, Toxicol. Vitr. 58 (2019) 110–117. https://doi.org/10.1016/j.tiv.2019.03.030.

[4] N. Li, Q. Jiang, F. Wang, J. Xie, Y. Li, J. Li, S. Wu, Emission behavior, environmental impact and priority-controlled pollutants assessment of volatile organic compounds (VOCs) during asphalt pavement construction based on laboratory experiment, J. Hazard. Mater. 398 (2020). https://doi.org/10.1016/j.jhazmat.2020.122904.

[5] A. Mizukoshi, K. Kumagai, N. Yamamoto, M. Noguchi, K. Yoshiuchi, H. Kumano, Y. Yanagisawa, A novel methodology to evaluate health impacts caused by VOC exposures using real-time VOC and Holter monitors, Int. J. Environ. Res. Public Health. 7 (2010) 4127–4138. https://doi.org/10.3390/ijerph7124127.

[6] P. Le Cloirec, COV (composés organiques volatils), Tech. l'Ingénieur. (2004).

[7] S. Sillman, The relation between ozone, NOx and hydrocarbons in urban and polluted rural environments, Atmos. Environ. 33 (1999) 1921–1845. https://doi.org/10.1016/S1474-8177(02)80015-8.

[8] P. Kuśtrowski, A. Rokicińska, T. Kondratowicz, Abatement of Volatile Organic Compounds Emission as a Target for Various Human Activities Including Energy Production, Adv. Inorg. Chem. 72 (2018) 385–419. https://doi.org/10.1016/bs.adioch.2018.05.004.

[9] M.S. Kamal, S.A. Razzak, M.M. Hossain, Catalytic oxidation of volatile organic compounds (VOCs) - A review, Atmos. Environ. 140 (2016) 117–134. https://doi.org/10.1016/j.atmosenv.2016.05.031.

[10] G. Avgouropoulos, E. Oikonomopoulos, D. Kanistras, T. Ioannides, Complete oxidation of ethanol over alkali-promoted Pt/Al_2O_3 catalysts, Appl. Catal. B Environ. 65 (2006) 62–69. https://doi.org/10.1016/j.apcatb.2005.12.016.

[11] L.F. Liotta, Catalytic oxidation of volatile organic compounds on supported noble metals, Appl. Catal. B Environ. 100 (2010) 403–412. https://doi.org/10.1016/j.apcatb.2010.08.023.

[12] V.P. Santos, S.A.C. Carabineiro, P.B. Tavares, M.F.R. Pereira, J.J.M. Órfão, J.L. Figueiredo, Oxidation of CO, ethanol and toluene over TiO_2 supported noble metal catalysts, Appl. Catal. B Environ. 99 (2010) 198–205. https://doi.org/10.1016/j.apcatb.2010.06.020.

[13] M.F. Finol, J. Rooke, B.L. Su, M. Trentesaux, J.M. Giraudon, J.F. Lamonier, Additional effects of Pt and Nb on hierarchically porous titania in the catalytic removal of n-butanol, Catal. Today. 192 (2012) 154–159. https://doi.org/10.1016/j.cattod.2011.11.004.

[14] H.L. Tidahy, M. Hosseni, S. Siffert, R. Cousin, J.F. Lamonier, A. Aboukaïs, B.L. Su, J.M. Giraudon, G. Leclercq, Nanostructured macro-mesoporous zirconia impregnated by noble metal for catalytic total oxidation of toluene, Catal. Today. 137 (2008) 335–339. https://doi.org/10.1016/j.cattod.2007.09.008.

[15] H.L. Tidahy, S. Siffert, J.F. Lamonier, E.A. Zhilinskaya, A. Aboukaïs, Z.Y. Yuan, A. Vantomme, B.L. Su, X. Canet, G. De Weireld, M. Frère, T.B. N'Guyen, J.M. Giraudon, G. Leclercq, New Pd/hierarchical macro-mesoporous ZrO_2, TiO_2 and ZrO_2-TiO_2 catalysts for VOCs total oxidation, Appl. Catal. A Gen. 310 (2006) 61–69. https://doi.org/10.1016/j.apcata.2006.05.020.

[16] M. Navlani-García, I. Miguel-García, Á. Berenguer-Murcia, D. Lozano-Castelló, D. Cazorla-Amorós, H. Yamashita, Pd/zeolite-based catalysts for the preferential CO oxidation reaction: Ion-exchange, Si/Al and structure effect, Catal. Sci. Technol. 6 (2016) 2623–2632. https://doi.org/10.1039/c5cy02044a.

[17] R. Sasikala, A.P. Gaikwad, V. Sudarsan, R. Rao, Jagannath, B. Viswanadh, S.R. Bharadwaj, The dual role of palladium in enhancing the photocatalytic activity of CdS dispersed on NaY-zeolite, Phys. Chem. Chem. Phys. 17 (2015) 6896–6904. https://doi.org/10.1039/c4cp06105e.

[18] M. Jabłońska, A. Król, E. Kukulska-Zajac, K. Tarach, V. Girman, L. Chmielarz, K. Góra-Marek, Zeolites Y modified with palladium as effective catalysts for low-temperature methanol incineration, Appl. Catal. B Environ. 166–167 (2015) 353–365. https://doi.org/10.1016/j.apcatb.2014.11.047.

[19] D. Verboekend, G. Vilé, J. Pérez-Ramírez, Hierarchical Y and USY Zeolites Designed by Post-Synthetic Strategies,

Adv. Funct. Mater. 22 (2012) 916–928. https://doi.org/10.1002/adfm.201102411.

[20] C.S. Cundy, P.A. Cox, The Hydrothermal Synthesis of Zeolites : History and Development from the Earliest Days to the Present Time, Chem. Rev. 103 (2003) 663–702. https://doi.org/10.1021/cr020060i.

[21] J. Zhu, Y. Cui, Y. Wang, F. Wei, Direct synthesis of hierarchical zeolite from a natural layered material w, Chem. Commun. (2009) 3282–3284. https://doi.org/10.1039/b902661d.

[22] Y. Li, J. Yu, New Stories of Zeolite Structures : Their Descriptions , Determinations , Predictions , and Evaluations, Chem. Rev. 114 (2014) 7268–7316. https://doi.org/10.1021/cr500010r.

[23] J. Zhao, Y. Yin, Y. Li, W. Chen, B. Liu, Synthesis and characterization of mesoporous zeolite Y by using block copolymers as templates, Chem. Eng. J. 284 (2016) 405–411. https://doi.org/10.1016/j.cej.2015.08.143.

[24] D. Verboekend, N. Nuttens, R. Locus, J. Van Aelst, P. Verolme, J.C. Groen, J. Pérez-Ramírez, B.F. Sels, Synthesis, characterisation, and catalytic evaluation of hierarchical faujasite zeolites: Milestones, challenges, and future directions, Chem. Soc. Rev. 45 (2016) 3331–3352. https://doi.org/10.1039/c5cs00520e.

[25] T. Ennaert, J. Van Aelst, J. Dijkmans, R. De Clercq, W. Schutyser, M. Dusselier, D. Verboekend, B.F. Sels, Potential and challenges of zeolite chemistry in the catalytic conversion of biomass, Chem. Soc. Rev. (2016) 584–611. https://doi.org/10.1039/c5cs00859j.

[26] W. Li, J. Zheng, Y. Luo, Z. Da, Effect of hierarchical porosity and phosphorus modification on the catalytic properties of zeolite Y, Appl. Surf. Sci. 382 (2016) 302–308. https://doi.org/10.1016/j.apsusc.2016.04.146.

[27] R.J. White, A. Fischer, C. Goebel, A. Thomas, A sustainable template for mesoporous zeolite synthesis, J. Am. Chem. Soc. 136 (2014) 2715–2718. https://doi.org/10.1021/ja411586h.

[28] J.J.F. Saceda, K. Rintramee, S. Khabuanchalad, S. Prayoonpokarach, R.L. de Leon, J. Wittayakun, Properties of zeolite Y in various forms and utilization as catalysts or supports for cerium oxide in ethanol oxidation, J. Ind. Eng. Chem. 18 (2012) 420–424. https://doi.org/10.1016/j.jiec.2011.11.108.

[29] O.S. Travkina, M.R. Agliullin, N.A. Filippova, A.N. Khazipova, I.G. Danilova, N.G. Grigor'Eva, N. Narender, M.L. Pavlov, B.I. Kutepov, Template-free synthesis of high degree crystallinity zeolite y with micro-meso-macroporous structure, RSC Adv. 7 (2017) 32581–32590. https://doi.org/10.1039/c7ra04742h.

[30] M. Zhu, L. Liang, H. Wang, Y. Liu, T. Wu, F. Zhang, Y. Li, I. Kumakiri, X. Chen, H. Kita, Influences of Acid Post-Treatment on High Silica SSZ-13 Zeolite Membrane, Ind. Eng. Chem. Res. 58 (2019) 14037–14043. https://doi.org/10.1021/acs.iecr.9b01250.

[31] Y. Wang, Y. Sun, C. Lancelot, C. Lamonier, J.C. Morin, B. Revel, L. Delevoye, A. Rives, Effect of post treatment on the local structure of hierarchical Beta prepared by desilication and the catalytic performance in Friedel-Crafts alkylation, Microporous Mesoporous Mater. 206 (2015) 42–51. https://doi.org/10.1016/j.micromeso.2014.12.017.

[32] R. Guo, Y. Qin, L. Qiao, J. Chen, X. Wu, Y. Yao, Enhancement of the catalytic performance in Pd-Cu/NaY catalyst for carbonylation of methyl nitrite to dimethyl carbonate: Effects of copper doping, Catal. Commun. 88 (2017) 94–98. https://doi.org/10.1016/j.catcom.2016.10.007.

[33] I. Rosso, C. Galletti, S. Fiorot, G. Saracco, E. Garrone, V. Specchia, Preferential CO oxidation over Pt/3A zeolite catalysts in H 2-rich gas for fuel cell application, J. Porous Mater. 14 (2007) 245–250. https://doi.org/10.1007/s10934-006-9060-8.

[34] L. Geng, J. Gong, G. Qiao, S. Ye, J. Zheng, N. Zhang, B. Chen, Effect of metal precursors on the performance of Pt/SAPO-11 catalysts for n-dodecane hydroisomerization, ACS Omega. 4 (2019) 12598–12605. https://doi.org/10.1021/acsomega.9b01216.

[35] N.M. Kinnunen, M. Suvanto, M.A. Moreno, A. Savimäki, K. Kallinen, T.J.J. Kinnunen, T.A. Pakkanen, Methane oxidation on alumina supported palladium catalysts: Effect of Pd precursor and solvent, Appl. Catal. A Gen. 370 (2009) 78–87. https://doi.org/10.1016/j.apcata.2009.09.018.

[36] P. Llewellyn, J. Rouquerol, L. Luciani, R. Denoyel, F. Rouquerol, Texture des matériaux pulvérulents ou poreux, Tech. l'Ingénieur. (2003).

[37] K. Bunmai, N. Osakoo, K. Deekamwong, W. Rongchapo, C. Keawkumay, N. Chanlek, S. Prayoonpokarach, J. Wittayakun, Extraction of silica from cogon grass and utilization for synthesis of zeolite NaY by conventional and microwave-assisted hydrothermal methods, J. Taiwan Inst. Chem. Eng. 83 (2018) 152–158. https://doi.org/10.1016/j.jtice.2017.11.024.

[38] S. Kulawong, N. Chanlek, N. Osakoo, Facile synthesis of hierarchical structure of NaY zeolite using silica from cogon grass for acid blue 185 removal from water, J. Environ. Chem. Eng. 8 (2020) 104114. https://doi.org/10.1016/j.jece.2020.104114.

[39] S. Oruji, R. Khoshbin, R. Karimzadeh, Preparation of hierarchical structure of Y zeolite with ultrasonic-assisted alkaline treatment method used in catalytic cracking of middle distillate cut: The effect of irradiation time, Fuel Process. Technol. 176 (2018) 283–295. https://doi.org/10.1016/j.fuproc.2018.03.035.

[40] C.K. Tsung, J.N. Kuhn, W. Huang, C. Aliaga, L.I. Hung, G.A. Somorjai, P. Yang, Sub-10 nm Platinum nanocrystals with size and shape control: Catalytic study for Ethylene and pyrrole hydrogenation, J. Am. Chem. Soc. 131 (2009) 5816–5822. https://doi.org/10.1021/ja809936n.

[41] H. Song, R.M. Rioux, J.D. Hoefelmeyer, R. Komor, K. Niesz, M. Grass, P. Yang, G.A. Somorjai, Hydrothermal growth of mesoporous SBA-15 silica in the presence of PVP-stabilized Pt nanoparticles: Synthesis, characterization, and catalytic properties, J. Am. Chem. Soc. 128 (2006) 3027–3037. https://doi.org/10.1021/ja057383r.

[42] V. V. Pushkarev, K. An, S. Alayoglu, S.K. Beaumont, G.A. Somorjai, Hydrogenation of benzene and toluene over size controlled Pt/SBA-15 catalysts: Elucidation of the Pt particle size effect on reaction kinetics, J. Catal. 292 (2012) 64–72. https://doi.org/10.1016/j.jcat.2012.04.022.

[43] Chunyu Chen, F. Chen, L. Zhang, S. Pan, C. Bian, X. Zheng, X. Meng, F. Xiao, Importance of platinum particle size for complete oxidation of toluene over Pt/ZSM-5 catalysts, Chem. Commun. 51 (2015) 5936–5938. https://doi.org/10.1039/b000000x.

[44] S. Liu, X. Wu, H. Luo, D. Weng, R. Ran, Pt/Zeolite Catalysts for Soot Oxidation: Influence of Hydrothermal Aging, J. Phys. Chem. C. 119 (2015) 17218–17227. https://doi.org/10.1021/acs.jpcc.5b04882.

[45] K. Pyra, K.A. Tarach, A. Śrębowata, I. Melián-Cabrera, K. Góra-Marek, Pd-modified beta zeolite for modulated hydro-cracking of low-density polyethylene into a paraffinic-rich hydrocarbon fuel, Appl. Catal. B Environ. 277 (2020) 119070. https://doi.org/10.1016/j.apcatb.2020.119070.

[46] M.P.S. Noah T. Plymale, Youn-Geun Kim, and N. Bruce S. Brunschwig, S. Lewis, Synthesis, Characterization, and Reactivity of Ethynyl- and Propynyl-Terminated Si(111) Surfaces, J Phys. Chem. 119 (2015) 19847–19862. https://doi.org/10.1021/acs.jpcc.5b05028.

[47] M.O. de Souza, F.M.T. Mendes, R.F. de Souza, J.H.Z. dos Santos, XPS characterization of nickel-acetylacetonate impregnated in NaX and NaY zeolites, Microporous Mesoporous Mater. 69 (2004) 217–221. https://doi.org/10.1016/j.micromeso.2003.12.001.

[48] V.K. Kaushik, M. Ravindranathan, X.p.s. study of copper-containing Y zeolites for the hydration of acrylonitrile to acrylamide, Zeolites. 12 (1992) 415–419. https://doi.org/10.1016/0144-2449(92)90039-R.

[49] X. Wang, K. Wang, C.A. Plackowski, A. V. Nguyen, Sulfuric acid dissolution of 4A and Na-Y synthetic zeolites and effects on Na-Y surface and particle properties, Appl. Surf. Sci. 367 (2016) 281–290. https://doi.org/10.1016/j.apsusc.2016.01.103.

[50] R.U. Islam, M.J. Witcomb, M.S. Scurrell, E. Van Der Lingen, W. Van Otterlo, K. Mallick, Conjugated polymer stabilized palladium nanoparticles as a versatile catalyst for Suzuki cross-coupling reactions for both aryl and heteroaryl bromide systems, Catal. Sci. Technol. 1 (2011) 308–315. https://doi.org/10.1039/c0cy00071j.

[51] K. McEleney, C.M. Crudden, J.H. Horton, X-ray photoelectron spectroscopy and the auger parameter as tools for characterization of silica-supported pd catalysts for the suzuki-miyaura reaction, J. Phys. Chem. C. 113 (2009) 1901–1907. https://doi.org/10.1021/jp808837k.

[52] X. Jiang, N. Koizumi, X. Guo, C. Song, Bimetallic Pd-Cu catalysts for selective CO_2 hydrogenation to methanol, Appl. Catal. B Environ. 170–171 (2015) 173–185. https://doi.org/10.1016/j.apcatb.2015.01.010.

[53] C. Dai, X. Li, A. Zhang, C. Liu, C. Song, X. Guo, Pd and Pd-CuO nanoparticles in hollow silicalite-1 single crystals for enhancing selectivity and activity for the Suzuki-Miyaura reaction, RSC Adv. 5 (2015) 40297–40302. https://doi.org/10.1039/c5ra05952f.

[54] Y. Dong, Y. Shen, Y. Zhao, S. Wang, X. Ma, Synergy between Palladium and Potassium Species for Efficient Activation of Carbon Monoxide in the Synthesis of Dimethyl Carbonate, ChemCatChem. 7 (2015) 2460–2466. https://doi.org/10.1002/cctc.201500317.

[55] J. Yang, W. Fan, C.M. Bell, Effect of calcination atmosphere on microstructure and H_2/CO_2 separation of palladium-doped silica membranes, Sep. Purif. Technol. 210 (2019) 659–669. https://doi.org/10.1016/j.seppur.2018.08.041.

[56] Z. Abdelouahab-Reddam, R. El Mail, F. Coloma, A. Sepúlveda-Escribano, Platinum supported on highly-dispersed ceria on activated carbon for the total oxidation of VOCs, Appl. Catal. A Gen. 494 (2015) 87–94. https://doi.org/10.1016/j.apcata.2015.01.026.

[57] J. Xu, X.C. Xu, L. Ouyang, X.J. Yang, W. Mao, J. Su, Y.F. Han, Mechanistic study of preferential CO oxidation on a Pt/NaY zeolite catalyst, J. Catal. 287 (2012) 114–123. https://doi.org/10.1016/j.jcat.2011.12.012.

[58] S.H. Park, M.S. Tzou, W.M.H. Sachtler, Temperature programmed reduction and re-oxidation of platinum in Y-zeolites, J. Chem. Inf. Model. 24 (1986) 85–98. https://doi.org/10.1016/S0166-9834(00)81259-2.

[59] K. Rintramee, K. Föttinger, G. Rupprechter, J. Wittayakun, Ethanol adsorption and oxidation on bimetallic catalysts containing platinum and base metal oxide supported on MCM-41, Appl. Catal. B Environ. 115–116 (2012) 225–235. https://doi.org/10.1016/j.apcatb.2011.11.050.

[60] J. Trawczyński, B. Bielak, W. Miśta, Oxidation of ethanol over supported manganese catalysts - Effect of the carrier, Appl. Catal. B Environ. 55 (2005) 277–285. https://doi.org/10.1016/j.apcatb.2004.09.005.

[61] F. Yin, S. Ji, P. Wu, F. Zhao, C. Li, Deactivation behavior of Pd-based SBA-15 mesoporous silica catalysts for the catalytic combustion of methane, J. Catal. 257 (2008) 108–116. https://doi.org/10.1016/j.jcat.2008.04.010.

[62] T. Barakat, J.C. Rooke, D. Chlala, R. Cousin, J.F. Lamonier, J.M. Giraudon, S. Casale, P. Massiani, B.L. Su, S. Siffert, Oscillatory behavior of Pd-Au catalysts in toluene total oxidation, Catalysts. 8 (2018) 1–11. https://doi.org/10.3390/catal8120574.

[63] S.C. Kim, W.G. Shim, Properties and performance of Pd based catalysts for catalytic oxidation of volatile organic compounds, Appl. Catal. B Environ. 92 (2009) 429–436. https://doi.org/10.1016/j.apcatb.2009.09.001.

[64] W.G. Shim, J.W. Lee, S.C. Kim, Analysis of catalytic oxidation of aromatic hydrocarbons over supported palladium catalyst with different pretreatments based on heterogeneous adsorption properties, Appl. Catal. B Environ. 84 (2008) 133–141. https://doi.org/10.1016/j.apcatb.2008.03.011.

[65] C. Chen, J. Zhu, F. Chen, X. Meng, X. Zheng, X. Gao, F.S. Xiao, Enhanced performance in catalytic combustion of toluene over mesoporous Beta zeolite-supported platinum catalyst, Appl. Catal. B Environ. 140–141 (2013) 199–205. https://doi.org/10.1016/j.apcatb.2013.03.050.

[66] J. Ying, H. Peng, X. Xu, R. Wang, F. Yu, Q. Sun, W. Liu, Z. Gao, X. Wang, Thermally stable ultra-small Pd nanoparticles encapsulated by silica: Elucidating the factors determining the inherent activity of noble metal catalysts, Catal. Sci. Technol. 6 (2016) 5405–5414. https://doi.org/10.1039/c6cy00201c.

[67] C. Chen, X. Wang, J. Zhang, S. Pan, C. Bian, L. Wang, F. Chen, X. Meng, X. Zheng, X. Gao, F.S. Xiao, Superior performance in catalytic combustion of toluene over KZSM-5 zeolite supported platinum catalyst, Catal. Letters. 144 (2014) 1851–1859. https://doi.org/10.1007/s10562-014-1295-4.

[68] Y. Hao, S. Chen, L. Wu, R. Chen, P. Sun, T. Chen, Hierarchically porous silica supported ceria and platinum nanoparticles for catalytic combustion of toluene, J. Alloys Compd. 867 (2021) 159030. https://doi.org/10.1016/j.jallcom.2021.159030.